1 Electronic Supplementary Information

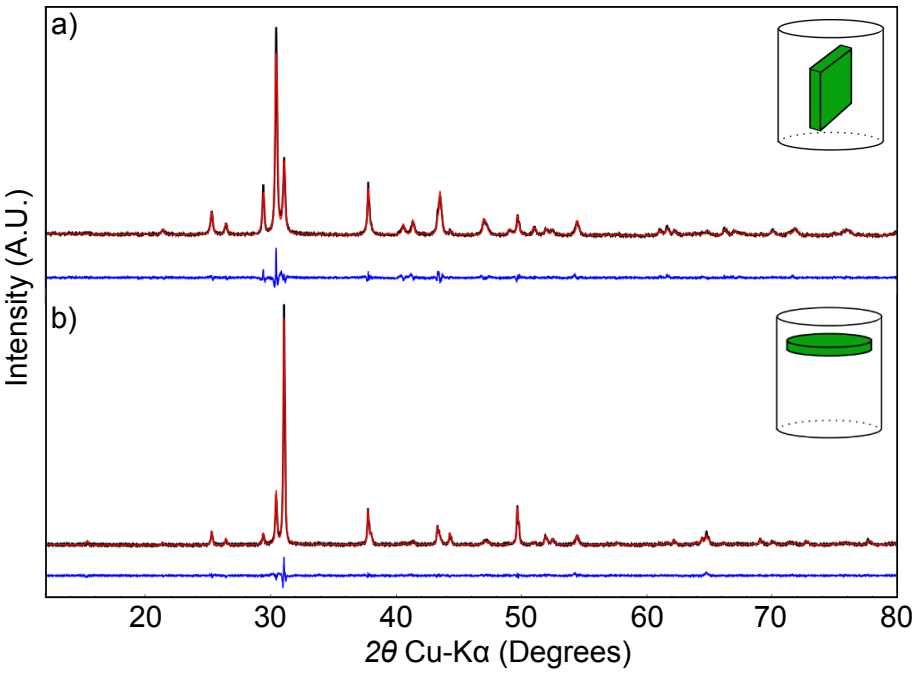

Figure S1 X-ray diffraction of pure, polycrystalline SnSe cut along different directions. a) Samples cut with primary face perpendicular to press direction are consistent with randomly textured polycrystalline SnSe. Rietveld fits (red) match experimental (black) data exceptionally well, confirming that the material is phase pure and of good crystalline quality. b)Samples cut with the primary face perpendicular to the press axis exhibit strong texturing in the (040) direction. Transport is expected to be anisotropic in SnSe, so textured samples are an additional complication we opted to avoid.

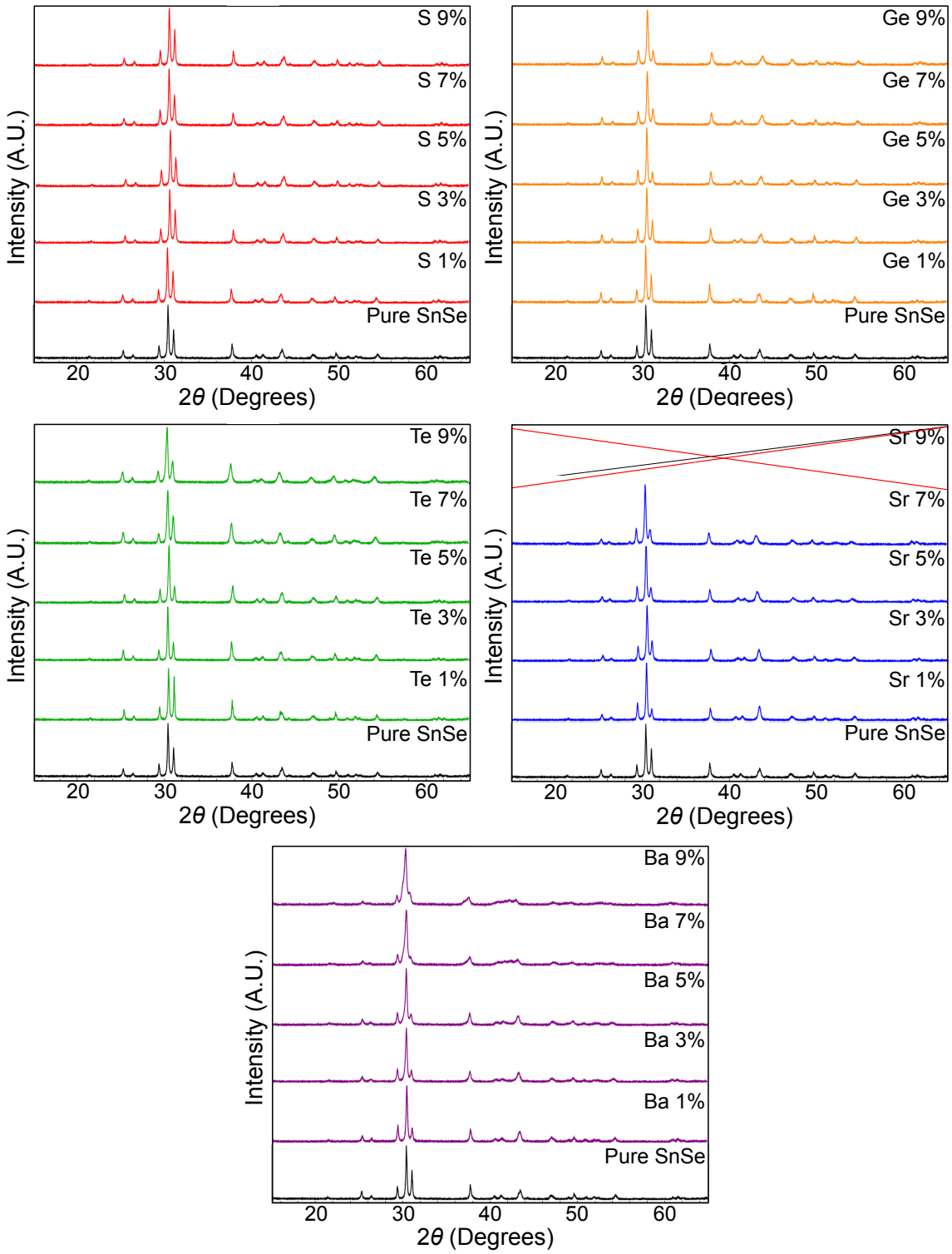

Figure S2 All X-ray diffraction patterns collected for alloyed plates of SnSe. Note that the 9 mol% Sr sample was not collected because phase separation was already observed at 7 mol%. Texturing is not completely consistent between all samples, but the degree of variation is relatively small with the exception of the 1 mol% Te sample. This is consistent with the discrepancy observed in the composition-dependent thermal conductivity measurement for the 1 mol% Te sample.

Table S1 Experimental speed of sound measurements performed on 5 mol% alloys of SnSe show no obvious trends. Errors shown represent 3σ from the mean value. Relatively large experimental error prohibits the significant conclusions from being drawn, particularly with regards to the effect of alloying species on the speed of sound.

Alloy	v_{shear} (m/s)	v_{long} (m/s)	v_{sound} (m/s)
SnSe	1330 ± 90	2020 ± 170	1560 ± 210
$SnSe_{0.95}\mathbf{S}_{0.05}$	1250 ± 49	1890 ± 180	1460 ± 190
$Sn_{0.95}\mathbf{Ge}_{0.05}Se$	1290 ± 50	1980 ± 140	1520 ± 160
$SnSe_{0.95}\mathbf{Te}_{0.05}$	1440 ± 75	2290 ± 140	1730 ± 180
$Sn_{0.95}\mathbf{Sr}_{0.05}Se$	1420 ± 22	2280 ± 66	1710 ± 73
$Sn_{0.95}\mathbf{Ba}_{0.05}Se$	1300 ± 21	2030 ± 67	1550 ± 74

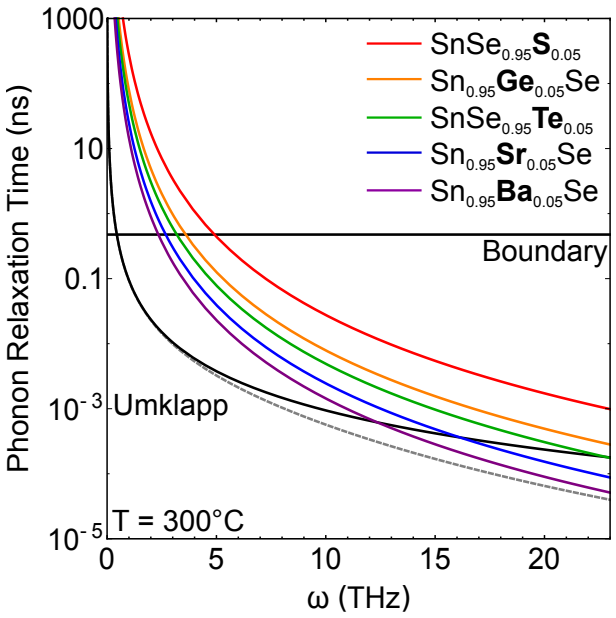

Figure S3 Curves illustrating the functional dependence of the phonon scattering terms τ_U, τ_B, and τ_{PD} on alloy species for 5 mol% samples. Umklapp and boundary scattering are fixed at values refined from pure SnSe. Notably, Umklapp scattering is the dominant scattering phenomenon in all systems except those containing Ba and Sr, in which point-defect scattering begins to dominate midway through the acoustic phonon frequencies. Boundary scattering contributes only weakly to the net relaxation time, generally dominated by Umklapp scattering except at very low phonon frequencies.

Table S2 Summary of some parameters of interest for all alloys after refinement with the Abeles model. Shown are ε, Γ_m, and Γ_s from the classical Abeles approach, the ratio of strain to mass scattering, and Γ_s'. Note that ε is composition *independent*, although all other parameters are explicitly dependent on composition by definition. The numerical value of ε is provided for transparency, although it is extremely sensitive to choice of radii and is not a numerically robust quantity. We note that the total and strain field scattering parameters track well with computational predictions.

Alloy	ε	Γ_m	Γ_s	Γ_{tot}	Γ_s/Γ_m	Γ_s'
S(1mol%)	0	0.0011	0	0.0011	0	0
S(3mol%)	0	0.0033	0	0.0033	0	0
S(5mol%)	0	0.0055	0	0.0055	0	0
S(7mol%)	0	0.0076	0	0.0076	0	0
S(9mol%)	0	0.0010	0	0.0010	0	0
Ge(1mol%)	14	0.0011	0.0019	0.0030	1.73	0.0013
Ge(3mol%)	14	0.0032	0.0055	0.0087	1.70	0.0038
Ge(5mol%)	14	0.0053	0.0089	0.0142	1.69	0.0063
Ge(7mol%)	14	0.0073	0.0122	0.0195	1.67	0.0087
Ge(9mol%)	14	0.0093	0.0154	0.0247	1.65	0.0110
Te(1mol%)	32	0.0012	0.0023	0.0035	1.92	0.0036
Te(3mol%)	32	0.0035	0.0068	0.0103	1.95	0.0104
Te(5mol%)	32	0.0056	0.0112	0.0168	1.99	0.0168
Te(7mol%)	32	0.0076	0.0154	0.0230	2.02	0.0230
Te(9mol%)	32	0.0095	0.0195	0.0290	2.06	0.0287
Sr(1mol%)	490	0.0005	0.0089	0.0094	18.0	0.0062
Sr(3mol%)	490	0.0015	0.0260	0.0275	17.9	0.0181
Sr(5mol%)	490	0.0024	0.0423	0.0447	17.8	0.0297
Sr(7mol%)	490	0.0033	0.0579	0.0612	17.6	0.0407
Sr(9mol%)	490	0.0042	0.0727	0.0769	17.5	0.0514
Ba(1mol%)	402	0.0002	0.0148	0.0441	84.4	0.0102
Ba(3mol%)	402	0.0005	0.0436	0.0275	84.7	0.0301
Ba(5mol%)	402	0.0008	0.0712	0.0720	85.0	0.0491
Ba(7mol%)	402	0.0011	0.0976	0.0987	85.3	0.0670
Ba(9mol%)	402	0.0014	0.1227	0.1241	85.6	0.0841

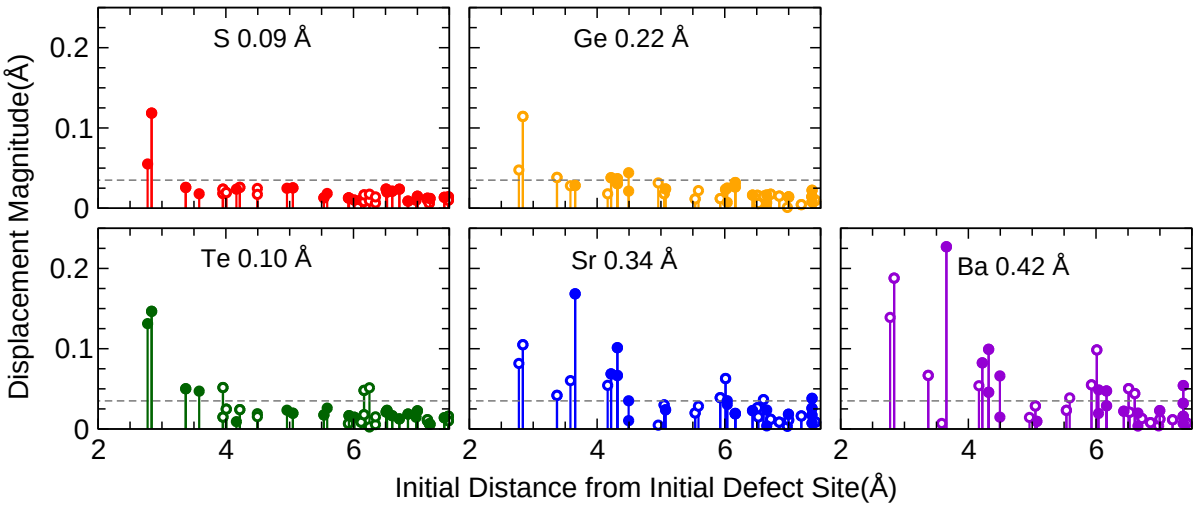

Figure S4 Distribution of the magnitude of individual atomic displacements from the Single Atom Distortion computational model. Filled circles denote Sn atoms, empty circles denote Se. The thermal cutoff, marked by the dashed gray line, indicates the threshold where computational error can no longer be distinguished from meaningful displacement data. This is most evident in the sulfur sample. We expect that the distortions near the sulfur defect should decay quickly as a function of distance from the defect, as SnS shares the same crystal structure an SnSe. Computationally, we observe several moderate distortions before the values plateau further from the defect site. We define the thermal cutoff slightly above the plateau, which is approximately 0.4Å. Similar behavior is observed for Ge and Te. Sr and Ba demonstrate stronger, more widely distributed defects, but are expected to plateau if a larger supercell is used.